J Mater Sci (2006) 41:5788–5792
DOI 10.1007/s10853-006-0121-9

LETTER

Fractograph–fatigue crack growth kinetics relationship for a fiber reinforced composite

Yong X. Gan · Heshmat A. Aglan

Received: 3 October 2005 / Accepted: 16 November 2005 / Published online: 13 May 2006

Fractography is widely used in post-failure analysis to identify fracture origin locations, stress characteristics and service environment. The fracture surface of filled polymer materials often provides clues to the initiation sites of crack, the growth mechanisms and the role of the reinforcement. The technique of scanning electron microscopy (SEM) is the most widely used method of studying fracture surface morphology. In addition, other techniques such as optical microscopy, transmission electron microscopy (TEM) and acoustic microscopy can provide useful complementary information. The SEM has been increasingly used for quantitative fractography in determination of mechanism of material failure. For polymeric and filled polymeric materials, the SEM serve as the key tool for evaluation of fracture surface features and the determination of failure mechanisms under either monotonic or cyclic tensile loading condition. The advantages of SEM include good depth of field and focus, and simple specimen preparation. The depth of focus is very important because both filled and unfilled polymeric materials display well-drawn and undulating nature of polymer chains under both overloading and cyclic loading conditions. This means that conventionally used optical microscopes are unable to capture the fracture surface features clearly because they are only in focus over a very limited small part of the cracking region. With SEM, it is possible to combine signals to create high resolution micrographs and yield different types of information (topographical, chemical, etc.).

In filled polymeric composites, crack propagation may occur by trans-filler fracture, interfacial debonding, and/or cohesive failure of the matrix. A number of studies have been conducted to determine the effect of varying the interfacial adhesion by selective treatment of the fillers. For example, Cantwell et al. [1] have studied the fracture surfaces of glass bead-filled resins. Commercial silane coupling agents used to improve the resin-filler adhesion. Also used were silicone-based mold release agents and other types of silane chemically incompatible with the epoxy resin to reduce the interfacial adhesion. It has been found that if the filler material is weak enough, the crack can pass directly through the particles. In some cases, the crack propagated around the particles. This effect has been reported for such fillers as aluminum trihydroxide [2], dolomite [3] and hollow glass spheres [4]. The toughening effect of the filler is also depends on the nature of filler/matrix interface.

Another important aspect which can influence the fracture mode, and hence the fracture surface morphology, is the crack speed. Young and Beaumont [5] have reported that the fracture surface morphology of a silica-filled epoxy resin changes at a threshold crack speed of 10^{-5} m/s. It has been found that above this value the cracks passed through the fillers. Below this speed, the crack propagation occurred by filler-matrix debonding and pull-out. Cantwell et al. [6] have also investigated the effect of crack speed on the fracture surface morphology. Double torsion tests were conducted on a silica-filled epoxy resin at various temperatures and crosshead displacement rates. The crack velocities (which were between 10^{-7} and 10^{-1} m/s) were measured by the graphite gauge technique. The resulting

Y. X. Gan (✉)
Department of Mechanical Engineering, Albert Nerken School of Engineering, The Cooper Union for the Advancement of Science and Art, 51 Astor Place, New York City, NY 10003, USA
e-mail: gan@cooper.edu

H. A. Aglan
Department of Mechanical Engineering, Tuskegee University, Tuskegee, AL 36088, USA

fracture surfaces were analyzed by using SEM. It has been found that the particles remain well-bonded to the matrix in the crack speeds of lower than10^{-6} m/s. Crack propagation along interface was also observed. The bonding-debonding threshold is a clear function of crack speed. Recent studies on the fracture and failure mechanisms of some of the filled polytetrafluoroethylene (PTFE) composites have also revealed the dependence of fracture surface morphology on the crack speed [7, 8].

In the present work, fatigue fractographic analysis of a fiber filled polymeric composite was performed, and correlation between the morphological features and fatigue crack propagation kinetics was made. The material is a 25% ceramic fiber filled PTFE. Such a polymeric composite possesses special properties such as resistance to wear, low thermal expansion, inert to chemicals, unaffected by outer space radiation, resistant to creep and cold flow. Thus, it has been recommended by NASA for applications in harsh environments including O-rings, gaskets, bearing liners etc. [9, 10]. Static tensile test were conducted on both unnotched and notched specimens for the evaluation of stress–strain relationship and residual tensile strength with a pre-crack. Such data are useful for choosing the fatigue test loading conditions including the maximum stress level, and stress ratio. Fatigue crack propagation test on the composite material was conducted under tension-tension cyclic loading at room temperature. In situ examination of the crack tip region during fatigue tests using a traveling optical microscope was performed. The crack length at different intervals was also measured during fatigue tests. Fractographic analysis was performed on fatigue fractured specimens. Various fracture regions were identified according to the morphological features.

Rectangular specimens for both static and fatigue tests were cut from the molded sheets with a thickness of 2.5 mm. The molded sheet was purchased from Tri-Star Plastics Corp., Charlotte, N.C. Specimens with a dimension of 60 mm × 12.5 mm were prepared for static tensile test. For fatigue tests, the specimens were cut into 152.4 mm in length and 25.4 mm in width. Single edge notch (SEN) specimens were prepared by introducing a cut at the center of one free edge of the specimens with a very sharp razor blade. The depth of the notch for static test specimens was 1.15 mm and 2.3 mm for fatigue test samples. The ratio of the notch depth to specimen width was kept the same as 0.09.

Both monotonic tensile and tension-tension fatigue tests were performed at room temperature using an 830 MTS hydraulic testing machine equipped with a 407 controller. A 4450 N load cell was used and the load range was set up from 0 to 445 N. Static tensile tests were performed under displacement control. The gauge length was 12.5 mm and the crosshead speed was 8×10^{-5} m/sec. A Yotogawa 3025 X-Y function recorder was used for drawing the load-displacement curves during testing, upon which stress–strain relationship for both notched and unnotched specimens from the material was established. Tension–tension fatigue tests were conducted under load control at a frequency of 3 Hz. The gauge length was kept at 100 mm. The applied maximum stress was 6 MPa, and the ratio of minimum stress to maximum stress was 0.1. The stress was calculated based on the original cross-sectional area before testing. The crack length at various intervals of number of cycles was recorded during the tests. An optical magnifier with a zoom lens was used to monitor the crack growth and to record the crack length. Fatigue crack propagation kinetics analysis was based on the data of crack length and number of cycles.

Typical samples from fatigue tests were chosen for microscopic observations. The fracture surfaces and associated damage zones were cut away from selected specimens and sputter coated with gold/palladium alloy using a Hummer 6.2 sputtering system manufactured by Anatech Ltd., Springfield, Virginia. The fracture surfaces and the side of damage zones were observed using a Hitachi S−2150 scanning electron microscope. All the micrographs were recorded on Polaroid 55 instant films.

The stress–strain curves for typical un-notched and notched tensile specimens are shown in Fig. 1. The material demonstrated an elastic behavior when the strain was less than 5%. After reached this strain value, the composite exhibited a nonlinear relationship between stress and strain. A plateau for the un-notched specimen occurred due to the cold flow of the PTFE matrix. The ultimate strength for the un-notched sample was 11 MPa, while the residual

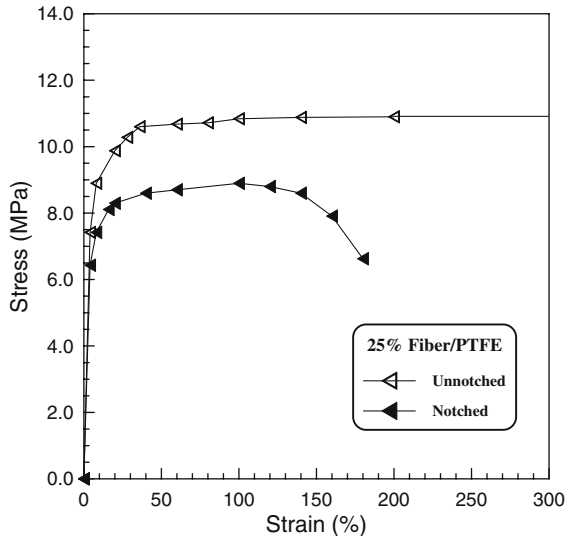

Fig. 1 Stress–strain relationship for both un-notched and notched specimens

strength for the notched sample is approximately 9 MPa. The strain to failure for notched sample was 180%.

The relationship between the crack length, a, and the number of cycles, N, for typical fatigue tested specimens was shown in Fig. 2. The initiation lifetime for this fiber filled PTFE materials was about 200,000 cycles and the lifetime of propagation reached about 800,000 cycles. The total fatigue lifetime for this material is 1,010,000 cycles. The slope of the curve in Fig. 2, as the average crack speed: da/dN, at each crack length, a, or at the corresponding number of cycles, N, was calculated. The relationship between da/dN and a for this material was shown in Fig. 3. The curve can be divided into three stages of fatigue crack propagation kinetics, i.e., initiation, stable propagation and unstable crack growth. The first stage; crack initiation, corresponds to the crack speed range from 1.0×10^{-10} m/cycle to 1.0×10^{-9} m/cycle. The stable crack propagation stage displayed crack speeds in the range from 2.0×10^{-9} m/cycle to 3.0×10^{-7} m/cycle. In the last stage, the crack moved very fast. The crack speed was found larger than 1.0×10^{-6} m/cycle. All these fatigue crack propagation stages will be correlated with the fracture surface features.

The morphology of fracture surface of a typical specimen tested under fatigue loading exhibited three distinct regions as schematically shown in Fig. 4; a region where crack initiation took place (region I), a stable crack propagation region (region II) and an unstable crack propagation region (region III). The first region is characterized by a lip of pulled-up matrix and demonstrates crack blunting and opening mechanisms. The characteristic features of region II are the large amount of ligament bundles and extensive fibrillation. The last region of unstable crack propagation showed a considerably smooth fracture surface. The above three regions are corresponding to the three fatigue crack growth stages as shown in Fig. 3.

The fatigue fracture surface morphology of the first region is shown in Fig. 5, a micrograph at 300×, taken from location ''A'' in Fig. 4. It can be seen from Fig. 5 that pull-out fibers (marked as ''a''), severely damaged matrix materials (marked as ''b'') with void coalescence (marked as ''c'') and ligament bundle formation (marked as ''d'') are the main features associated with the crack initiation. These bundles were severely drawn indicative of considerable plastic deformation of the matrix associated with the crack blunting and plastic flow of the matrix along the crack move direction. The crack can be observed propagated in an irradiated way as indicated by the fan-shaped distribution of both the ligaments and the fibers. A few of ligaments with a considerably large size can be found with the tip split into more and finer fibrils. Such a feature can be found at the upper right corner in the same micrograph of Fig. 5. Fiber filler can be observed in the regularly drawn-out area. Along the lower edge of Fig. 5, the damaged matrix can be seen full of voids aligned in the crack propagation direction. Most of these voids formed due to the fiber/matrix debonding and fiber pulled-out.

The fracture surface features of region II revealed a high energy consuming process associated with the stable crack propagation. This is evidenced by the extensive plastic

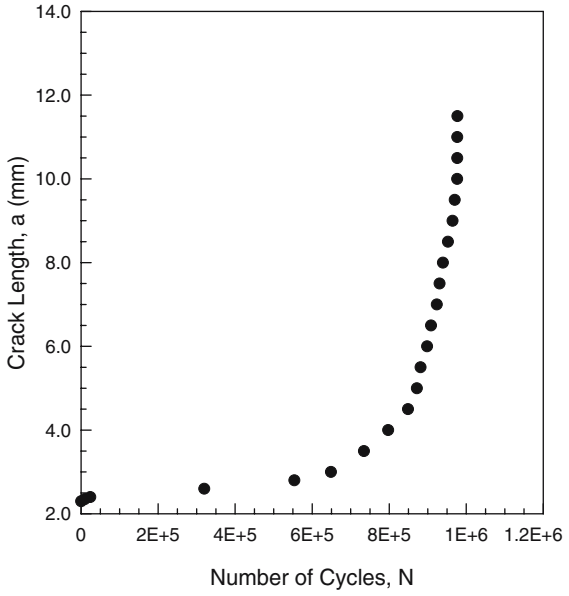

Fig. 2 Relationship between the crack length, a, and the number of cycles, N, for a fatigue tested specimen of the 25% fiber reinforced PTFE composite material

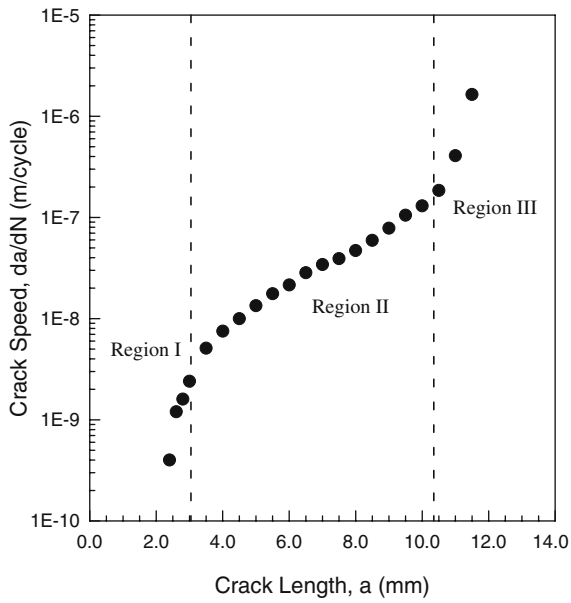

Fig. 3 Relationship between the crack speed, da/dN, and the crack length, a, for a typical fatigue specimen showing three different stages of fatigue crack propagation kinetics, i.e., crack initiation, stable crack propagation and unstable crack growth

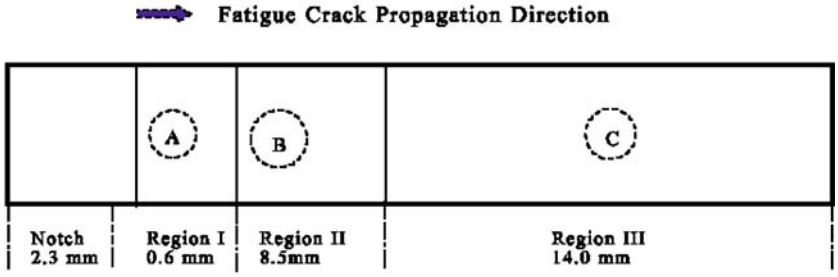

Fig. 4 Schematic illustration showing three different regions on the fatigue fracture surface; crack initiation, stable crack propagation and unstable crack growth. Also shown are the locations for microscopic examination

deformation and severe fibrillation of the matrix as shown in Fig. 6, a micrograph at 300×, taken from location ''B'' in Fig. 4. Most part of the fracture surface is covered with ligaments or fibrils (marked as ''a'' and ''b'', respectively). The fiber fillers (marked as ''c'') are found below these features. Some of these fibers were pulled out and aligned along the crack propagation direction. Unlike the second region, the critical crack growth region; region III, displays a brittle-like crack growth mechanism. Fiber pull-out is the major fracture surface feature. The PTFE matrix shows very limited deformation, as can be seen from Fig. 7, a micrograph at 300×, taken from location ''C'' in Fig. 4. It can also be seen from this micrograph that the surface is full of voids (marked as ''a''). The undrawn matrix separated by tearing (marked as ''b'') can be seen in some areas. From the tearing direction of the matrix, it can be seen that the main crack moved from left hand side to right hand side, and the existence of fiber filler served as secondary crack initiator and main crack deviator. In some locations, the bridging effect of these fibers (marked as ''c'') caused the change in the propagation directions of those secondary cracks. Since no fibrillation can be found,

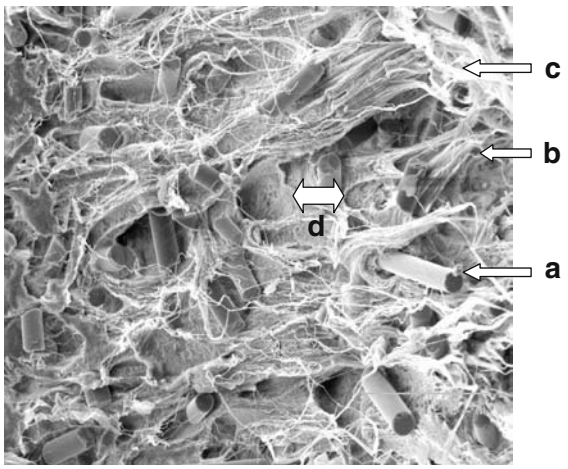

Fig. 5 Micrograph at 300× showing the fracture surface of the first region. Damaged matrix with voids aligned in the crack propagation direction can be observed. Ligament bundles were severely pulled up with the crack initiation. In some particular area, the crack can be seen propagated in an irradiated way. Such feature was imprinted on the fractured matrix as shown in the upper right corner of the micrograph

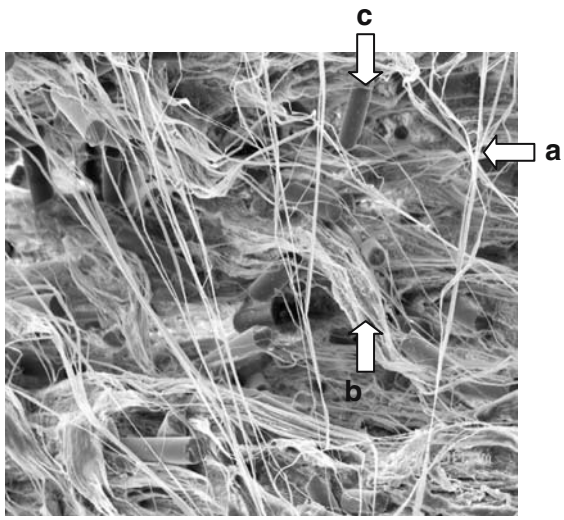

Fig. 6 Micrograph at 300× showing the fracture surface features of region II. Most part of the surface is covered with ligaments or fibrils. The extensive plastic deformation and severe fibrillation reveal a high energy consuming process. Ductile failure mechanism can be found related to the crack stable propagation

such fracture surface morphology revealed a fast tearing failure mechanism in the last stage of fatigue crack growth.

The active zone of the fiber reinforced PTFE was also identified by microscopic examination. As known, during

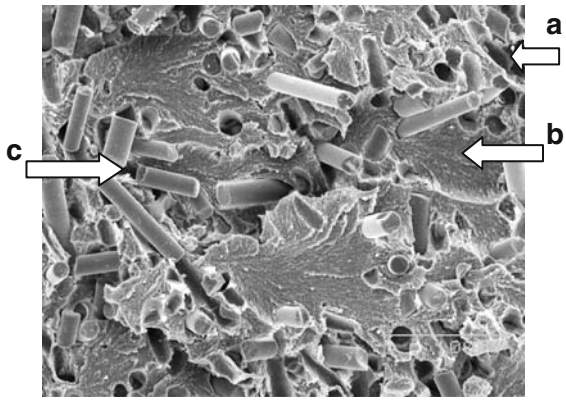

Fig. 7 Micrograph at 300× showing the fracture surface morphology of region III. Fiber pull-out and very limited plastic deformation of the matrix are the major fracture surface features indicative of a fast crack growth process in the last stage

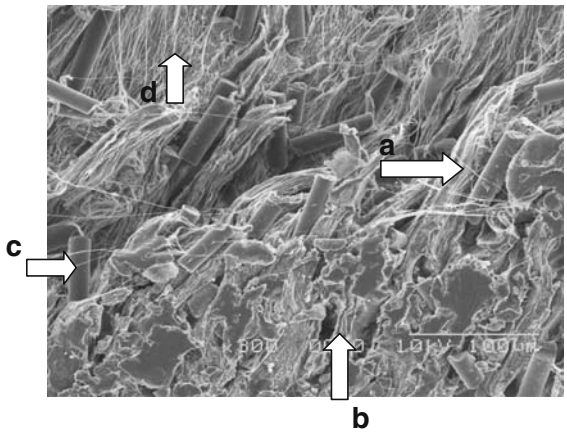

Fig. 8 Micrograph at 300× showing the area containing the boundary of the side zone and the fracture surface. Ligament bundles, discontinuity, fibrillation, matrix drawn-up and void can be seen in the active zone

the fatigue damage process, an active zone within crack layer can form [11, 12]. This damage zone can be identified from a side-view of the specimen as shown in Fig. 8, a micrograph at 300×, taken from the side damage zone near the notch tip. In Fig. 8, the lower right part stands for the side view of the damage zone. The upper left section of the micrograph is a tilted view of the fracture surface. Obviously, shear band (marked as ''a'') and a lot of micro-discontinuities (marked as ''b'') were formed associated with the fatigue crack growth. Damage features such as fiber pull-out (marked as ''c''), matrix crazes and plastic flow inside the active zone (marked as ''d'') can be clearly seen from the same micrograph.

Acknowledgments The experimental part of this work was in part sponsored by NASA John F. Kennedy Space Center under contract number NAG10−0168 through Tuskegee University. The technical guidance of P. D. Faughnan and C. Bryan of Materials Science Division, NASA Kennedy Space Center is also acknowledged.

References

1. Cantwell WJ, Roulin-Moloney AC (1989) In: Roulin-Moloney AC (ed) Fractography and failure mechanisms of polymers and composites, Elsevier Applied Science, London, New York, p 241
2. Lange FF, Radford KC (1971) J Mater Sci 6:1197
3. Moloney AC, Kausch HH, Stieger HR (1983) J Mater Sci 18:208
4. Moloney AC, Kausch HH, Stieger HR (1984) J Mater Sci 19:1125
5. Young RJ, Beaumont PWR (1975) J Mater Sci 10:1343
6. Cantwell WJ, Roulin-Moloney AC, Kaiser T (1988) J Mater Sci 23:1615
7. Zhang Z, Aglan H, Faughnan P, Bryan C (1998) J Reinforced Plastics and Composites 17:752
8. Aglan H, Gan Y, El-Hadik M, Faughnan P, Bryan C (1999) J Mater Sci 34:83
9. Aglan H (1996) NASA Technical Annual Report, NASA John F. Kennedy Space Center, Florida, p 10
10. Aglan H (1997) NASA Technical Annual Report, NASA John F. Kennedy Space Center, Florida, p 2
11. Aglan H (1993) Int J Damage Mech 2:53
12. Aglan H, Gan Y (2001) J Mater Sci 36:389